第38卷第6期 2022年6月
无 机 化 学 学 报 CHINESE JOURNAL OF INORGANIC CHEMISTRY
Vol.38 No.6 1189-1198

用于高性能锂硫电池的二维氮硫共掺杂多孔碳纳米片的快速合成

孙 林[#,1,2] 谢 杰[#,2,3] 程 峰[*,2] 陈若愚[*,3] 朱庆莉[*,4] 金 钟[*,1]
([1]南京大学化学化工学院,教育部介观化学重点实验室,配位化学国家重点实验室,南京 210023)
([2]盐城工学院化学化工学院,江苏省新型重点环保实验室,盐城 224051)
([3]常州大学材料科学与工程学院,常州 213164)
([4]金陵科技学院理学院,南京 210009)

摘要: 本工作基于工业炼油产品沥青,开发了一种无金属、氮和硫共掺杂多孔碳纳米片(NSPC)的合成方法。获得的多孔碳纳米片具有高比表面积(339 $m^2 \cdot g^{-1}$)和优异的固硫能力。同时,高含量氮、硫共掺杂可以有效增强碳材料的导电性,同时促进多硫化物的高效催化转化。通过熔融法固硫后,制备得到的NSPC/S电极具有较高的比容量和优异的循环稳定性(在0.6C电流密度下,200次循环后容量为762 $mAh \cdot g^{-1}$),实现了高含量氮和硫共掺杂的二维多孔碳材料的快速批量生产并用于高性能锂硫电池正极材料。

关键词: 多孔碳; 二维材料; 硫阴极; 模板法; 锂硫电池
中图分类号: O613.61; O613.51 **文献标识码:** A **文章编号:** 1001-4861(2022)06-1189-10
DOI: 10.11862/CJIC.2022.116

Rapid Construction of Two-Dimensional N, S-Co-doped Porous Carbon for Realizing High-Performance Lithium-Sulfur Batteries

SUN Lin[#,1,2] XIE Jie[#,2,3] CHENG Feng[*,2] CHEN Ruo-Yu[*,3] ZHU Qing-Li[*,4] JIN Zhong[*,1]
([1]*School of Chemistry and Chemical Engineering, Key Laboratory of Mesoscopic Chemistry, Ministry of Education, State Key Laboratory of Coordination Chemistry, Nanjing University, Nanjing* 210023, *China*)
([2]*School of Chemistry and Chemical Engineering, Key Laboratory for Advanced Technology in Environmental Protection of Jiangsu Province, Yancheng Institute of Technology, Yancheng, Jiangsu* 224051, *China*)
([3]*School of Materials Science and Engineering, Changzhou University, Changzhou, Jiangsu* 213164, *China*)
([4]*School of Science, Jinling University of Science and Technology, Nanjing* 210009, *China*)

Abstract: In this work, based on the industrial refinery product of pitch, we have developed a simple method for the production of metal-free, nitrogen, and sulfur co-doping porous carbon nanosheets (NSPC). The obtained NSPC exhibited a high specific surface area (339 $m^2 \cdot g^{-1}$) and puissant adsorbability for sulfur fixation. At the same time, the co-doping of N and S can effectively improve the electrical conductivity of carbon nanomaterials, and further improve the adsorption and conversion reaction of lithium polysulfides (LIPSs). The NSPC/S electrode delivered superior cycling performance (762 $mAh \cdot g^{-1}$ at 0.6C after 200 cycles). This work represents a rapid and massive production of two-dimensional porous carbon materials with high content of N and S as the cathode for advanced lithium-sulfur batteries.

Keywords: porous carbon; two-dimensional material; sulfur cathode; template method; lithium-sulfur battery

收稿日期:2022-03-10。收修改稿日期:2022-04-26。
中央高校基本科研业务费(No.0205-14380266, 0205-14380272)、国家重点研发计划(No.2017YFA0208200)、国家自然科学基金(No.22022505,21872069)、江苏省碳达峰碳中和专项资金(No.BK20220008)、2021年苏州姑苏科技创业领军人才计划、盐城工学院人才引进项目(No.xjr2019006)、江苏省新型环保重点实验室开放课题、江苏省高校自然科学基金(No.20KJD530003)和金陵科技学院孵化项目(No.jit fhxm 201922)资助。
[#]共同第一作者。
[*]通信联系人。E-mail:zhongjin@nju.edu.cn,chry@cczu.edu.cn,zhuqingli@jit.edu.cn

0 Introduction

Since the commercialization in the 1990s, the application of lithium-ion batteries (LIBs) caused great changes in relation to the realm of energy storage and conversion[1]. With the rapid development of electric vehicles, and the continuously increasing public demands, the energy density of current LIBs is approaching the limit. Seeking batteries with higher energy density and power density, as well as prolonged lifespans is extremely important. Compared with LIBs, lithium-sulfur (Li-S) batteries with the configuration of metallic Li anode and sulfur cathode have a high theoretical capacity (1 675 $mAh \cdot g^{-1}$) and energy density (2 567 $Wh \cdot kg^{-1}$) and are widely regarded as one of the most promising electrochemical energy storage devices[2-3]. For Li-S battery systems, it is generally accepted that the reversible reactions between S_8 molecules and the metallic Li anode enable the steady charge/discharge process. However, the product of lithium polysulfides (LiPSs) derived from the discharge shows superior solubility in common organic electrolytes, the formed soluble long-chain LiPS species will shuttle from the cathode to the anode, and the further reduced short-chain LiPSs (Li_2S_2 and Li_2S) will be deposited[4-5]. The so-called "shuttle effect" is adverse to the fixation of sulfur and capacity retention. Additionally, the inherent insulative of sulfur and sulfides, as well as the non-negligible volume expansion (*ca.* 78%) during the charging-discharging process, severely hinder the real-world application[6].

To address the aforementioned issues, one of the most effective strategies is to develop advanced sulfur host materials that simultaneous acting as sulfur carriers and promoters for the accelerated electrocatalytic conversion of LiPSs[7-13]. For an applicable host material, the following material design principles should be included: First, the host material should possess excellent electronic conductivity, which can enable the rapid migration of electrons, thereby improving the rate capabilities; Second, the superior physical confinement, the chemical affinity, as well as the effective catalytic conversion of LiPSs are combined in a competent host material for sulfur fixation; Third, the large specific surface area or abundant inner cavities of the host material can accommodate more elemental sulfur and alleviate the volume expansion, as well as enable the exposure of more catalytically active sites to boosting the overall performances of Li-S batteries.

Pure carbon as a sulfur host can limit the dissolution of LiPSs by simple physical adsorption. However, the electroneutrality of pure carbon materials is generally non-polar, and intermolecular interactions with polar intermediates during charge and discharge are weak. The good cycling and rate performance of Li-S cells are largely dependent on good contact between carbon and sulfur and the excellent wettability of the electrolyte. In addition, the abundant polysulfide traps of sulfur at the interface mitigate the dissolution of polysulfides during the electrochemical process, avoiding shuttle effects, and improving the utilization of polysulfides. The number of active sites will be determined by the surface properties of the carbon materials at the interface, which has an impact on polysulfide adsorption. Therefore, various strategies have been developed to optimize interfaces with fast electron/ion transfer and sufficient active sites. For example, functional groups can improve the polarity of non-polar carbon-based materials, which can help to improve the interfacial immersion of carbon/sulfur electrodes in the electrolyte and enable close contact through the formation of bonds between carbon and sulfur (*i.e.*, C—S and S—O). In addition, polar functional groups can provide chemically active sites for polysulfides through strong polar interactions and effectively limit the shuttling of polysulfides from the anode to the cathode. Therefore, the rational design of optimized interfaces in nanostructured carbon/sulfur materials would provide a new way to improve the performance of Li-S batteries. Thus, heteroatom-doped (*e.g.*, oxygen (O), nitrogen (N), and boron (B)) carbon materials are chemically fabricated or derived from the residues of carbonaceous precursors[14-18]. For instance, nitrogen-doped carbon materials are used to improve the polarity and conductivity of the carbon materials interface in Li-S cells through their different chemical environments with pyridine N, graphite N, and pyrrole N[19-21]. Compared to pure car-

bon materials, the carbon with N-functional groups exhibited a high discharge capacity of 1 100 $mAh \cdot g^{-1}$ (0.35 $mA \cdot cm^{-2}$) and relative cycling stability at a multiplicity of 0.70 $mA \cdot cm^{-2}$ [22]. It is believed that the electroactive N-functional groups in the carbon composites can effectively trap LiPSs by forming chemical bonds with lithium ions during the electrochemical process.

In this work, we design and synthesize two-dimensional (2D) metal-free, N and S co-doped porous carbon (NSPC) nanosheets. The petrochemical-derived pitch, melamine, and porous MgO were utilized as the carbon skeleton, the nitrogen source, and the hard template, respectively. An N, S co-doped 2D carbon nanoporous sheet with high specific surface area and micropores can be obtained through a simple calcination treatment. The formed unique structure can accommodate more elemental sulfur and relieve the volume expansion during the charge and discharge process. Concurrently, the micropores that existed on the surface of the carbon nanosheets can improve the wettability of the electrolyte and improve the cycle performance and the introduction of N and S atoms are beneficial for the fixation of LiPSs. Compared with traditional carbon-sulfur composite materials, 2D NSPC nanosheets showed better electrochemical performance and cycle stability when used as lithium-sulfur battery cathodes.

1 Experimental

1.1 Synthesis of porous MgO template

Typically, purchased MgO powder was mixed with deionized water with ultrasonic agitation. The formed mixture was boiled for 24 h in a reflux apparatus. The obtained material was calcined at 500 ℃ for 30 min after filtration and drying to afford porous MgO.

1.2 Synthesis of 2D NSPC

In a typical synthesis, the pitch powder, porous MgO template, and melamine were uniformly mixed in ethanol in the proportion of 1∶1∶1 in weight. After continuous stirring and drying in an oven at 80 ℃, a grey powder mixture was obtained. The powder was then crushed and calcined in a quartz tube under 700 ℃ for 30 min with argon protection. The obtained black powder was treated with a hydrochloric acid solution (1 $mol \cdot L^{-1}$). After washing and drying, the hierarchical porous carbon material doped with N and S named NSPC was finally obtained. For comparison, S-doped porous carbon (SPC) was prepared by treating the mixture of MgO and pitch (1∶1 in weight) as above.

1.3 Synthesis of metal-free NSPC/S

Typically, 60 mg of NSPC and 240 mg of sulfur were ground in the agate mortar for 30 min. The mixture was sealed in a pasteurized glass tube and heated at 155 ℃ for 10 h in an oven. The obtained product was marked as NSPC/S. For comparison, SPC/S with the same weight ratio of sulfur was also prepared by the same method using SPC.

1.4 Polysulfide adsorption test

Li_2S_6 solution was prepared by mixing sublimed sulfur and Li_2S with a molar ratio of 5∶1 in 1,2-dimethoxyethane (DME) and 1,3-dioxolane (DOL) (1∶1 in volume) solution. The stirring was then done at 60 ℃ for 12 h until the powders were completely dissolved and the solution turned yellow. A Li_2S_6 solution with a concentration of 3 $mmol \cdot L^{-1}$ was used. 20 mg of NSPC and SPC were added to 4 mL of the Li_2S_6 solution, separately. Then, the mixture was vigorously stirred to obtain thorough adsorption, and a glass vial filled with the bare Li_2S_6 solution served as the blank sample.

1.5 Characterizations

Powder X-ray diffraction (PXRD) was performed on an X′Pert3 Powder instrument (PANalytical, Netherland) using a Cu $K\alpha$ radiation (λ=0.154 16 nm) at an operating voltage of 40 kV and current of 40 mA with scanning range of 5°-90°. Scanning electron microscopy (SEM) was conducted on a Nova NanoSEM 450 field-emission scanning electron microscope at acceleration voltages of 15 kV. Transmission electron microscopy (TEM) and energy-dispersive X-ray spectroscopy (EDS) was carried out using a JEM-1400-plus instrument (Japan) at acceleration voltages of 200 kV. Atomic force microscopy (AFM) was conducted using a SPI3800/SPA400 instrument (Seiko Inc., Japan). Raman spectroscopy (InVia-Reflex, Renishaw) was performed with a laser source of 633 nm wavelength. X-ray photoelectron spectroscopy (XPS) data were collected with an ESCALAB 250Xi (Thermo Fisher Scientific). Nitrogen

adsorption-desorption tests were carried out at 77 K using Micrometrics ASAP 2020 analyzer after vacuum degassing of the samples at 120 ℃ for 8 h. The thermogravimetric analysis (TGA) was conducted on a STA499f5 analyzer at a heating rate of 10 ℃·min^{-1}. The ultraviolet-visible (UV-Vis) spectra were obtained on a Hitachi U-3900H UV-Vis spectrophotometer.

1.6 Electrochemical measurements

Coin cells (CR2025) were employed to evaluate the electrochemical performance of the obtained NSPC/S product. The assembly process was performed in an Ar gas-filled glove box with both H_2O and O_2 lower than 10^{-7}. The active material, conductive graphite, and polyvinylidene fluoride (PVDF) binder was fixed at a mass ratio of 8∶1∶1. The formed slurry was stirred in deionized water and blade-coated on an Al foil with a coarse surface. After drying at 50 ℃ in a vacuum for 10 h, the coated Al foil was cut into disks 12 mm in diameter. The electrolyte consisted of a solution of 1.0 mol·L^{-1} lithium bis(trifluoromethanesulfonyl)imide (LiTFSI) and 1.0% $LiNO_3$ in a mixture of DME/DOL with a volume ratio of 1∶1, and a Celgard 2400 film was used as the separator. The counter electrode was pure Li slices. The charge-discharge tests were performed on a Neware battery testing system (Shenzhen, China) at the constant current mode in the voltage range of 1.7-2.8 V. The specific capacities were calculated based on the total weight of active materials. The loading weight of active material was fixed at *ca*. 1.0 mg·cm^{-2}. For comparison, SPC/S electrodes were also prepared in the same way. The electrochemical impedance spectroscopy (EIS) was recorded on an electrochemical workstation (CHI660E, Chenhua, CHN) with a range of 100 kHz to 0.01 Hz over the entire frequency range.

1.7 Theoretical calculations

Theoretical calculations based on density functional theory (DFT) were performed in this work by using the Vienna *ab initio* simulation package (VASP). The projector-augmented-wave (PAW) potentials were adopted while the generalized gradient approximations (GGA) of Perdew-Burke-Ernzerhof (PBE) pseudopotentials were applied for the exchange-correlation functional[23-24]. The Li_2S_n (n=1, 2, 4, 6, 8) adhesion binding energy (E_b) was calculated using the formula of $E_b = E_{NSPC/S} - E_{NSPC} - E_{Li_2Sn}$, where $E_{NSPC/S}$ is the total energy of the adsorbed system, E_{NSPC} is the total energy of the surface, and E_{Li_2Sn} is the total energy of the isolated Li_2S_n polysulfide. Herein, more negative values demonstrate the possibility of adsorbate-surface interactions due to the energy advantage.

2 Results and discussion

As shown in Fig.1a, NSPC/S was synthesized via a facile two-step method. Firstly, the pitch, melamine, and porous MgO were uniform mixed, with facile annealing and pickling, and NSPC was attained. Fig. S1a and S1b (Supporting information) show the morphology of NSPC, which exhibits the typical hierarchical features. NSPC is composed of closely assembled nanoplatelets. The EDS analysis (Fig. S1c) of NSPC also displays the atomic fractions of doped N and S were 1.06% and 0.68%, respectively. Fig. 1b displays the elemental mapping results of NSPC, which show the presence of C, N, and S elements. Herein, as shown in Fig.S2a, the MgO powders used in this work exhibited porous sheet-like structures, and regular lattice fringes with a d-spacing of 0.152 nm were further confirmed with high-resolution transmission electron microscopy (HRTEM). As shown in Fig.S2b, the insert Fourier transform diffraction explicitly demonstrates the exposure of the (220) lattice plane of MgO[12]. Secondly, NSPC/S was prepared through a typical melt-diffusion strategy with elemental sulfur. As illustrated, NSPC/S in Fig. S1d maintained the initial morphology of NSPC/S, and no aggregated sulfur particle was observed on the surface. The elemental mapping results (Fig. S1d) show the presence of C and S elements, demonstrating the homogeneous distribution of sulfur in NSPC. The thickness of the ultrathin structures was investigated by AFM measurements, which are presented in Fig. S3. The average thickness of the obtained NSPC was calculated as 1-3 nm, implying that a large lateral-to-thickness ratio is very beneficial for electron mobility.

PXRD analysis was employed to investigate the crystalline phase of the prepared samples. As illustrat-

ed in Fig. 2a, the PXRD patterns of both NSPC and graphite showed a sharp peak at approximately 25° and another weak peak at approximately 44°, which can be assigned to the typical (002) and (100) planes of carbon, respectively. Moreover, compared with graphite, it should be noted that the peak location of the (002) plane for NSPC was slightly lower, signifying enlarged d-spacing[25], which is consistent with the TEM results. At the same time, the broadened peak width of NSPC also confirms the very thin structures. The Raman spectrum of NSPC is presented in Fig. 2b, showing the D band at 1 340 cm^{-1} (defects) and the G band at 1 580 cm^{-1} (crystalline graphite)[26]. The peak intensity ratio of the D to G band (I_D/I_G) was 3.2, implying the presence of abundant defects in NSPC. In addition, the XPS technique was employed to investigate the chemical states and elemental ratios of N and S. The survey XPS spectrum of NSPC is shown in Fig.2c. Only elements of C, O, N, and S can be detected, and the atomic fractions of N and S were 9.5% and 1.7%, respectively. The C1*s* XPS spectrum of NSPC is shown in Fig. 2d. The deconvolution can be mainly divided into two peaks: a sharp peak at 284.7 eV (C—C bond) and a broad peak at approximately 286.0 eV (C—O, C—N, *etc.*) [27]. The higher N content compared to the EDS results implies that the doped N is mostly adsorbed on

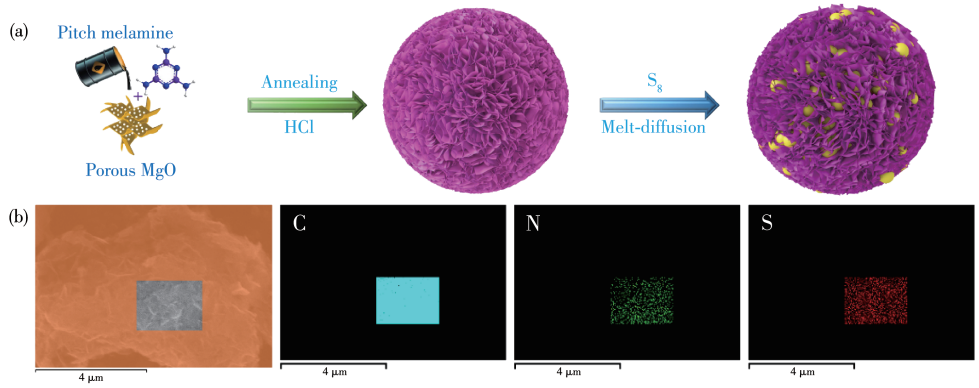

Fig.1　(a) Schematic illustration showing the preparation of NSPC and NSPC/S; (b) SEM image and mappings of NSPC

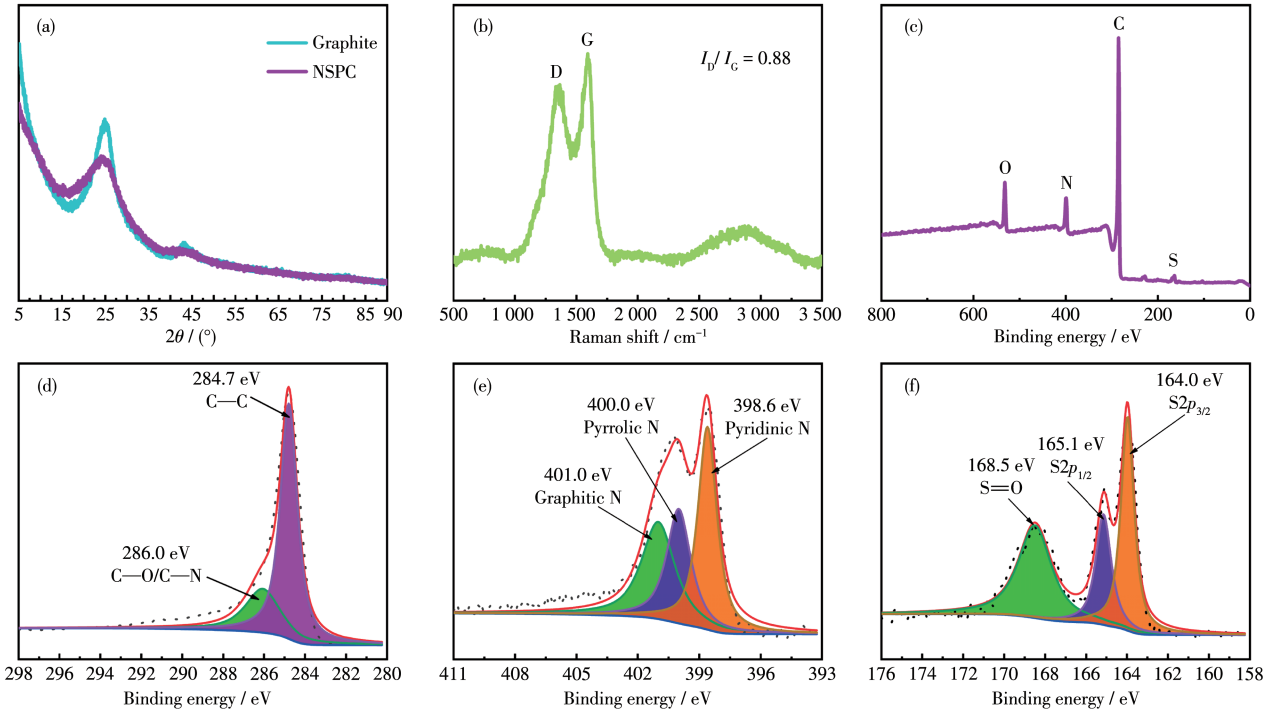

Fig.2　(a) XRD patterns of graphite and NSPC; (b) Raman spectra and (c) survey, (d) C1*s*, (e) N1*s*, and (f) S2*p* XPS spectra of NSPC

the surface of NSPC. Fig.2e shows the N1*s* XPS spectrum of the NSPC nanosheets, and the peaks located at 398.6, 400.0, and 401.0 eV are attributed to pyridinic N, pyrrolic N, and graphitic N, respectively[28]. The ratio of pyridinic N, pyrrolic N, and graphitic N was estimated to be 1∶0.74∶0.84. Concurrently, graphitic N with three sp^2 carbon atoms plays an important role in improving the conductivity of graphitic carbon[29-30]. Besides, the pyridinic N and pyrrolic N promote the catalytic conversion of LiPSs effectively[16-18]. Therefore, in this work, the contents of different types of N can achieve a good balance while considering the capacity and rate performance of the NSPC electrodes. Fig. 2f exhibits the S2*p* XPS spectrum of NSPC, and the peaks at 164.0 and 165.1 eV can be assigned to S2$p_{3/2}$ and 2$p_{1/2}$, indicating that most of the S are integrated into the graphite matrix[31]. Additionally, the S2*p* XPS spectrum of NSPC contained a peak at 168.5 eV, which is attributed to oxidized S[32].

Moreover, the adsorption - desorption isotherms and pore size distributions of NSPC and SPC are shown in Fig. 3a, 3b, and Fig. S4a, S4b, respectively. Fig. 3a and Fig. S4a show that the sorption isotherm can be indexed to type Ⅳ with an H1 hysteresis loop and Brunauer-Emmett-Teller (BET) surface area of 339 and 522 $m^2 \cdot g^{-1}$ for NSPC and SPC, respectively; these results indicate the presence of mesopores in the structure. The H1 hysteresis loop indicates that both NSPC and SPC have clearly narrow pore size distributions, as illustrated in Fig.3b and Fig.S4b. The pore size distributions of approximately 6.5 and 8 nm for NSPC and SPC were observed using the Barrett-Joyner-Halenda (BJH) model for analysis. The narrow pore size distribution is likely linked to the porous MgO template. Meanwhile, the reduced BET surface area and pore size for NSPC are mainly ascribed to the introduction of melamine. Therefore, the large specific surface area and suitable pore size facilitate the efficient storage of more sulfur.

In addition, N elemental doping effectively improves the adsorption capacity of the NSPC/S electrode to LiPSs, which can be seen from the polysulfides adsorption test in Fig.4a and 4b. Besides, the accurate sulfur content in NSPC/S was determined by the TGA result under N_2 atmosphere from room temperature to 700 ℃. As presented in Fig.4c, owing to a large number of pores and high pore volume of NSPC/S, the sulfur content (mass fraction) in NSPC/S can be as high as *ca*. 68%. When employed as sulfur cathode for Li-S batteries, NSPC/S with porous nanostructures, highly electrical conductive channels, and strong chemisorption capability with sulfur species can effectively alleviate the issues caused by the low electrical conductivity of sulfur and the severe shuttle effect of polysulfides.

To investigate the electrochemical behaviors of the synthesized sample, a CR2025 coin-like half-cell was employed with a pure Li plate as a counter electrode to evaluate the electrochemical performance. For comparisons, the control sample of SPC/S was also examined under the same experimental conditions. The detailed cell assembly process is presented in the Experimental Section. The first three cycles of the

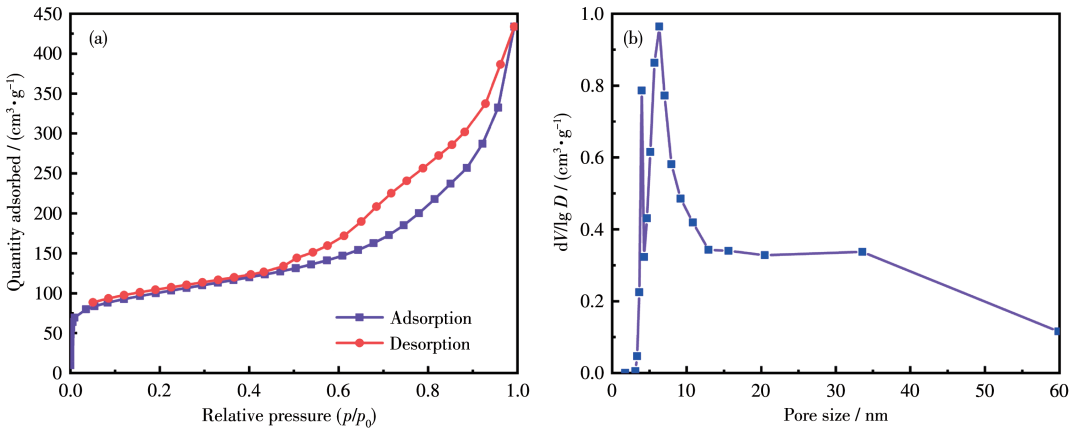

Fig.3 (a) N_2 adsorption-desorption isotherm, and (b) pore size distribution of NSPC

cyclic voltammetry (CV) curves of the NSPC/S electrode at a scan rate of 0.2 mV·s^{-1} in the voltage range of 1.5 and 3.0 V (vs Li/Li$^+$) are shown in Fig.4e. In the first cathodic scan, the reduction peaks at 2.2 and 1.7 V correspond to Li_2S_6 or Li_2S_4 and insoluble Li_2S_2 and Li_2S products, respectively[33]. In addition, in the first anode scan, the oxidation peak at 2.5 V should be ascribed to the oxidation of Li_2S to S_8[34]. In the next two scans, the positions of the oxidation and reduction peaks shifted, indicating that the redox reaction of the battery was improved and the full contact between electrolyte and electrode.

Fig.4f presents the last discharge-charge voltage profiles of the NSPC/S electrode at different current densities. As the current increased, the voltage hysteresis (ΔE) of the NSPC/S electrode increased gradually. And the ΔE of NSPC/S (Fig.4f) was smaller than that of SPC/S at 0.1C (Fig.S5), implying the reaction kinetics rate was improved, which accounts for the better electrochemical performance at high current densities.

Furthermore, the rate performance of the NSPC/S electrode is shown in Fig. 4g. Notably, the electrode was activated at a low current density for several cycles before testing. The NSPC/S electrode delivered high specific capacities of 1 176, 1 032, 761, 626, 415, and 153 mAh·g^{-1} at current densities of 0.1C, 0.2C, 0.6C, 1C, 2C, and 4C, respectively. Importantly, the NSPC/S electrode exhibited good reversibility, with the specific discharge capacity recovering to the initial value while the current density returns to 0.1C. For comparison,

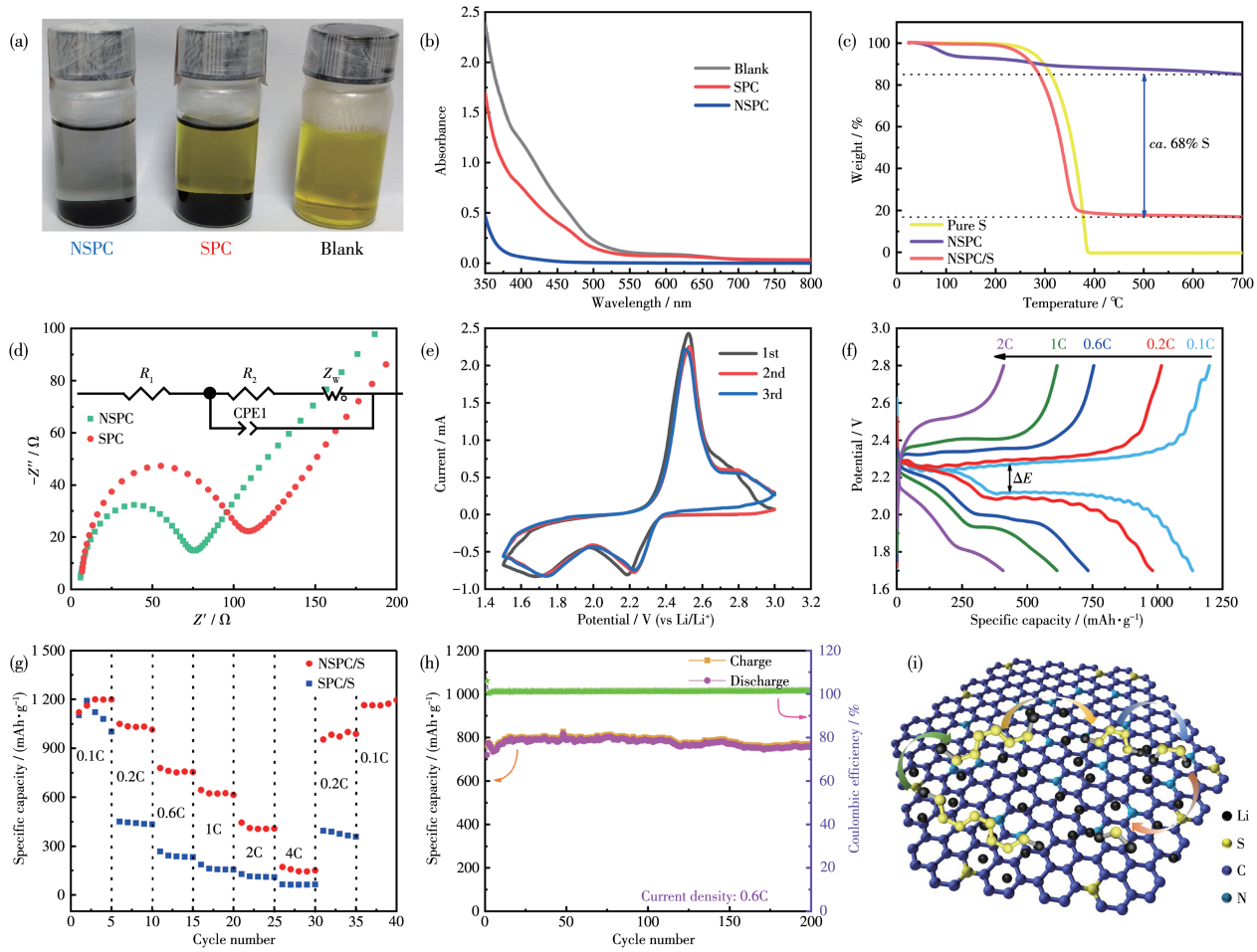

Fig.4　(a) Optical photo of the adsorption effect of NSPC and SPC on Li_2S_6; (b) UV-Vis spectra of NSPC and SPC; (c) TGA of pure S, NSPC, and NSPC/S; (d) EIS curves of NSPC and SPC; (e) CV curves of NSPC/S from 3.0 to 1.5 V (vs Li/Li$^+$) at a scan rate of 0.2 mV·s^{-1}; (f) Voltage profiles of NSPC/S electrodes at various current densities; (g) Rate performance of NSPC/S electrodes; (h) Cycling performance of NSPC/S electrodes at high current densities; (i) Schematic diagram of the catalytic conversion of LiPSs

the SPC/S electrode without doped N only delivered 1 099, 442, 243, 163, 114, and 63 mAh·g^{-1} at the same current densities listed above. Hence, the doped N plays an important role in enhancing the rate performance of NSPC/S electrodes. As shown in Fig.4d, the NSPC/S electrode exhibited a lower internal resistance than that of SPC/S, indicating that doped graphitic N enables higher conductivity. The illustration in Fig.4d is the equivalent circuit diagram of the EIS, R_1 stands for solution resistance, R_2 stands for charge transfer resistance, Z_W stands for diffusion resistance, and CPE1 stands for capacitive reactance.

The long-term cycling stability of NSPC/S and SPC/S electrodes is shown in Fig.4h. At the little current density of 0.1C (Fig.S6), the NSPC/S cathode also provided 1 185 mAh·g^{-1} after 50 cycles. And at the high current density of 2C, the NSPC/S cathode retained a reversible capacity of 463 mAh·g^{-1} after 200 cycles (Fig.S7), which is significantly higher than that of SPC/S (157 mAh·g^{-1}). In addition, the NSPC/S cathode delivered an outstanding cycling performance, which provided 762 mAh·g^{-1} at 0.6C after 200 cycles. Moreover, a stable Coulombic efficiency (CE) of >99% was achieved throughout the long-term cycling, confirming the high S utilization, excellent LiPSs confinement, and good reversibility of LiPSs conversion of NSPC/S. Compared with the SPC/S electrode material without N doping, the electrode capacity attenuates faster, and the shuttle effect of LiPSs affects the long-term cycle stability of the battery.

The catalytic conversion of LiPSs with pyridinic N, pyrrolic N, S^1, and S^2 (different S substitution positions in the graphene host, as shown in Fig. S8) are shown in Fig.4i. To shed more light on the functional mechanism, the interactions between the series of NSPC and polysulfides Li_2S_n ($2\leqslant n\leqslant 8$) were investigated by first-principles DFT calculations. For pyridinic N, pyrrolic N, S^1, and S^2, the relevant calculation results are shown in Fig.5 and Fig.S8. It was concluded from the calculations that pyridinic N has the highest adsorption energy to Li_2S_n ($2\leqslant n\leqslant 8$). Hence, the electrochemical performance of SPC without nitrogen doping is much lower than NSPC.

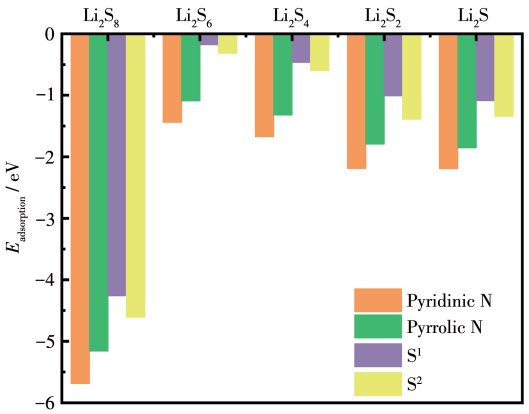

Fig.5 Adsorbability of pyrrolic N, pyridinic N, and S^1 and S^2 of Li_2S_n (n=1, 2, 4, 6, and 8)

3 Conclusions

In summary, we propose a facile synthesis method for the production of N, S co-doped carbon nanomaterial, which features 2D nanostructures. After sulfur fixation, it still retains the previous morphologies. The doped N can effectively improve the electrical conductivity of the material and the adsorption capacity of LiPSs. The electrochemical performance of NSPC/S has been greatly improved when compared with pure graphite, which is mainly ascribed to the doped N and S and also confirmed by the theoretical calculation. The NSPC/S electrode delivered a superior rate capability (415 mAh·g^{-1} at 2C) and an outstanding cell performance (762 mAh·g^{-1} at 0.6C after 200 cycles, 463 mAh·g^{-1} at 2C after 200 cycles). The promotion of polysulfides transformation with NSPC demonstrates that synergizing strong polysulfides adsorption and superior electronic conductivity is critical for the rational design of cathode materials in Li-S batteries. Furthermore, this work provides a novel strategy to synthesize 2D N doped porous carbon nanomaterial for realizing advanced Li-S batteries.

Conflicts of interest: There are no conflicts to declare.

Supporting information is available at http://www.wjhxxb.cn

References:

[1]Yoshino A. The Birth of the Lithium-Ion Battery. *Angew. Chem. Int.*

Ed., **2012**,**51**:5798-5800

[2]Lim W G, Kim S, Jo C, Lee J. A Comprehensive Review of Materials with Catalytic Effects in Li-S Batteries: Enhanced Redox Kinetics. *Angew. Chem. Int. Ed.*, **2019**,**58**:18746-18757

[3]Evers S, Nazar L F. New Approaches for High Energy Density Lithium-Sulfur Battery Cathodes. *Acc. Chem. Res.*, **2013**,**46**:1135-1143

[4]Lu Y, Qin J L, Shen T, Yu Y F, Chen K, Hu Y Z, Liang J N, Gong M X, Zhang J J, Wang D L. Hypercrosslinked Polymerization Enabled N-Doped Carbon Confined Fe_2O_3 Facilitating Li Polysulfides Interface Conversion for Li-S Batteries. *Adv. Energy Mater.*, **2021**,**11**:2101780

[5]Li W T, Guo X T, Geng P B, Du M, Jing Q L, Chen X D, Zhang G X, Li H P, Xu Q, Braunstein P, Pang H. Rational Design and General Synthesis of Multimetallic Metal-Organic Framework Nano-Octahedra for Enhanced Li-S Battery. *Adv. Mater.*, **2021**,**33**:2105163

[6]Wang N N, Zhang X, Ju Z Y, Yu X W, Wang Y X, Du Y, Bai Z C, Dou S X, Yu G H. Thickness-Independent Scalable High-Performance Li-S Batteries with High Areal Sulfur Loading via Electron-Enriched Carbon Framework. *Nat. Commun.*, **2021**,**12**:4519

[7]Zhang S L, Ao X, Huang J, Wei B, Zhai Y L, Zhai D, Deng W Q, Su C L, Wang D S, Li, Y D. Isolated Single-Atom Ni-N_5 Catalytic Site in Hollow Porous Carbon Capsules for Efficient Lithium-Sulfur Batteries. *Nano Lett.*, **2021**,**21**:9691-9698

[8]Luo D, Li C J, Zhang Y G, Ma Q Y, Ma C Y, Nie Y H, Li M, Weng X F, Huang R, Zhao Y, Shui L L, Wang X, Chen Z W. Design of Quasi-MOF Nanospheres as a Dynamic Electrocatalyst toward Accelerated Sulfur Reduction Reaction for High-Performance Lithium-Sulfur Batteries. *Adv. Mater.*, **2021**,**34**:2105541

[9]Wang T, Luo D, Zhang Y G, Zhang Z, Wang J Y, Cui G L, Wang X, Yu A P, Chen Z W. Hierarchically Porous Ti_3C_2 MXene with Tunable Active Edges and Unsaturated Coordination Bonds for Superior Lithium-Sulfur Batteries. *ACS Nano*, **2021**,**15**:19457-19467

[10]Wang M L, Sun Z T, Ci H N, Shi Z X, Shen L, Wei C H, Ding Y F, Yang X Z, Sun J Y. Identifying the Evolution of Selenium-Vacancy-Modulated $MoSe_2$ Precatalyst in Lithium-Sulfur Chemistry. *Angew. Chem. Int. Ed.*, **2021**,**60**:24558-24565

[11]Qian T, Huang Y C, Zhang M D, Xia Z Z, Liu H Y, Guan L, Hu H, Wu M B. Non-corrosive and Low-Cost Synthesis of Hierarchically Porous Carbon Frameworks for High-Performance Lithium-Ion Capacitors. *Carbon*, **2021**,**173**:646-654

[12]Guan L, Hu H, Li L Q, Pan Y Y, Zhu Y F, Li Q, Guo H L, Wang K, Huang Y C, Zhang M D, Yan Y C, Li Z T, Teng X L, Yang J W, Xiao J Z, Zhang Y N, Wang X S, Wu M B. Intrinsic Defect-Rich Hierarchically Porous Carbon Architectures Enabling Enhanced Capture and Catalytic Conversion of Polysulfides. *ACS Nano*, **2020**,**14**:6222-6231

[13]Guan L, Pan L, Peng T Y, Qian T, Huang Y C, Li X X, Gao C, Li Z, Hu H, Wu M B. Green and Scalable Synthesis of Porous Carbon Nanosheet-Assembled Hierarchical Architectures for Robust Capacitive Energy Harvesting. *Carbon*, **2019**,**152**:537-544

[14]Park S K, Lee J K, Kang Y C. Yolk-Shell Structured Assembly of Bamboo-like Nitrogen-Doped Carbon Nanotubes Embedded with Co Nanocrystals and Their Application as Cathode Material for Li-S Batteries. *Adv. Funct. Mater.*, **2018**,**28**:1705264

[15]Xu J, Lawson T, Fan H B, Su D W, Wang G X. Updated Metal Compounds (MOFs, -S, -OH, -N, -C) Used as Cathode Materials for Lithium-Sulfur Batteries. *Adv. Energy Mater.*, **2018**,**8**:1702607

[16]Mi K, Chen S W, Xi B J, Kai S S, Jiang Y, Feng J K, Qian Y T, Xiong S L. Sole Chemical Confinement of Polysulfides on Nonporous Nitrogen/Oxygen Dual-Doped Carbon at the Kilogram Scale for Lithium-Sulfur Batteries. *Adv. Funct. Mater.*, **2017**,**27**:1604265

[17]Zhang L L, Wan F, Wang X Y, Cao H M, Dai X, Niu Z Q, Wang Y J, Chen J. Dual-Functional Graphene Carbon as Polysulfide Trapper for High-Performance Lithium Sulfur Batteries. *ACS Appl. Mater. Interfaces*, **2018**,**10**:5594-5602

[18]Peng Y Y, Zhang Y Y, Huang J X, Wang Y H, Li H, Hwang B J, Zhao J B. Nitrogen and Oxygen Dual-Doped Hollow Carbon Nanospheres Derived from Catechol/Polyamine as Sulfur Hosts for Advanced Lithium Sulfur Batteries. *Carbon*, **2017**,**124**:23-33

[19]Zhou W D, Wang C M, Zhang Q L, Abruña, H D, He Y, Wang J W, Mao S X, Xiao X C. Tailoring Pore Size of Nitrogen-Doped Hollow Carbon Nanospheres for Confining Sulfur in Lithium-Sulfur Batteries. *Adv. Energy Mater.*, **2015**,**5**:1401752

[20]Lin T Q, Chen I. W, Liu F X, Yang C Y, Bi H, Xu F F, Huang F Q. Nitrogen-Doped Mesoporous Carbon of Extraordinary Capacitance for Electrochemical Energy Storage. *Science*, **2015**,**350**:1508-1513

[21]Song J X, Gordin M L, Xu T, Chen S R, Yu Z X, Sohn H, Lu J, Ren Y, Duan Y H, Wang, D H. Strong Lithium Polysulfide Chemisorption on Electroactive Sites of Nitrogen-Doped Carbon Composites For High-Performance Lithium-Sulfur Battery Cathodes. *Angew. Chem. Int. Ed.*, **2015**,**54**:4325-4329

[22]Song J X, Xu T, Gordin M L, Zhu P Y, Lv D P, Jiang Y B, Chen Y S, Duan Y H, Wang D H. Nitrogen-Doped Mesoporous Carbon Promoted Chemical Adsorption of Sulfur and Fabrication of High-Areal-Capacity Sulfur Cathode with Exceptional Cycling Stability for Lithium-Sulfur Batteries. *Adv. Funct. Mater.*, **2014**,**24**:1243-1250

[23]Blöchl P E. Projector Augmented-Wave Method. *Phys. Rev. B*, **1994**, **50**:17953-17979

[24]Perdew J P, Burke K, Ernzerhof M. Generalized Gradient Approximation Made Simple. *Phys. Rev. Lett.*, **1996**,**77**:3865-3868

[25]Zhao Y C, Liu Z, Chu W G, Song L, Zhang Z X, Yu D L, Tian Y J, Xie S S, Sun L F. Large-Scale Synthesis of Nitrogen-Rich Carbon Nitride Microfibers by Using Graphitic Carbon Nitride as Precursor. *Adv. Mater.*, **2008**,**20**:1777-1781

[26]Kesavan D, Mariappan V K, Krishnamoorthy K, Kim S J. Carbothermal Conversion of Boric Acid into Boron-Oxy-carbide Nanostructures for High-Power Supercapacitors. *J. Mater. Chem. A*, **2021**,**9**:915-921

[27]Wang X, Wang J, Wang D L, Dou S, Ma Z L, Wu J H, Tao L, Shen A L, Ouyang C B, Liu Q H, Wang S Y. One-Pot Synthesis of Nitrogen and Sulfur Co-doped Graphene as Efficient Metal-Free Electrocatalysts for the Oxygen Reduction Reaction. *Chem. Commun.*, **2014**,**50**: 4839-4842

[28]Zhou Y J, Zhang L X, Huang W M, Kong Q H, Fan X Q, Wang M,

Shi J L. N-Doped Graphitic Carbon-Incorporated g-C_3N_4 for Remarkably Enhanced Photocatalytic H_2 Evolution under Visible Light. *Carbon*, **2016**,**99**:111-117

[29]Lei W, Xiao W P, Li J D, Li G R, Wu Z X, Xuan C J, Luo D, Deng Y P, Wang D L, Chen Z W. Highly Nitrogen-Doped Three-Dimensional Carbon Fibers Network with Superior Sodium Storage Capacity. *ACS Appl. Mater. Interfaces*, **2017**,**9**:28604-28611

[30]Zhu Y E, Yang L P, Zhou X L, Li F, Wei J P, Zhou Z. Boosting the Rate Capability of Hard Carbon with an Ether-Based Electrolyte for Sodium Ion Batteries. *J. Mater. Chem. A*, **2017**,**5**:9528-9532

[31]Klingele M, Pham C, Vuyyuru K R, Britton B, Holdcroft S, Fischer A, Thiele S. Sulfur Doped Reduced Graphene Oxide as Metal-Free Catalyst for the Oxygen Reduction Reaction in Anion and Proton Exchange Fuel Cells. *Electrochem. Commun.*, **2017**,**77**:71-75

[32]Yang S B, Zhi L J, Tang K, Feng X L, Maier J, Müllen K. Efficient Synthesis of Heteroatom (N or S)-Doped Graphene Based on Ultrathin Graphene Oxide-Porous Silica Sheets for Oxygen Reduction Reactions. *Adv. Funct. Mater.*, **2012**,**22**:3634-3640

[33]Peng L L, Wei Z Y, Wan C Z, Li J, Chen Z, Zhu D, Baumann D, Liu H T, Allen C S, Xu X, Kirkland A I, Shakir I, Almutairi Z, Tolbert S, Dunn B, Huang Y, Sautet P, Duan X F. A Fundamental Look at Electrocatalytic Sulfur Reduction Reaction. *Nat. Catal.*, **2020**,**3**:762-770

[34]Zhang H, Yang L, Zhang P G, Lu C J, Sha D W, Yan B Z, He W, Zhou M, Zhang W, Pan L, Sun Z M. MXene-Derived Ti_nO_{2n-1} Quantum Dots Distributed on Porous Carbon Nanosheets for Stable and Long-Life Li-S Batteries: Enhanced Polysulfide Mediation via Defect Engineering. *Adv. Mater.*, **2021**,**33**:2008447